Fall 12-15-2017

# Effect of Metal Ion Substitution on Electrochemical Properties of Cobalt Oxide for Energy Applications

Dalal Alqahtani
*Pittsburg State University*, dalqahtani@gus.pittstate.edu

# EFFECT OF METAL ION SUBSTITUTION ON ELECTROCHEMICAL PROPERTIES OF COBALT OXIDE FOR ENERGY APPLICATIONS

A Thesis Submitted to the Graduate School
in Partial Fulfillment of the Requirements
for The Degree of
Master of Science

Dalal Alqahtani

Pittsburg State University

Pittsburg, Kansas

December, 2017

EFFECT OF METAL ION SUBSTITUTION ON ELECTROCHEMICAL PROPERTIES OF COBALT OXIDE FOR ENERGY APPLICATIONS

Dalal Alqahtani

APPROVED:

Thesis Advisor_____
Dr. Ram Gupta, Department of Chemistry

Committee Member _____
Dr. Khamis Siam, Department of Chemistry

Committee Member _____
Dr. Pawan Kahol, Department of Physics

Committee Member _____
Dr. John Franklin, Department of English and Modern Languages

ACKNOWLEDGEMENTS

First of all, I would like to thank my family and friends, especially my father and mother for their trust, support, and encouragement. Also, I would thank my country, Saudi Arabia, who afforded this great opportunity for me.

I would like to sincerely thank my advisor, Dr. Ram Gupta, for his guidance and teaching, as well as his understanding of many things that helped me to have a comfortable working environment and his assistance in achieving this work successfully.

Additionally, I would like to thank my committee members, Dr. Khamis Siam, Dr. Pawan Kahol, and Dr. John Franklin, as well as other faculty members in the Chemistry Department at Pittsburg State University. In addition, I would like to thank Dr. Sanjay Mishra, at the University of Memphis, for recording SEM images.

EFFECT OF METAL ION SUBSTITUTION ON ELECTROCHEMICAL PROPERTIES OF COBALT OXIDE FOR ENERGY APPLICATIONS

An Abstract of the Thesis by
Dalal Alqahtani

Metal oxides are being used for various applications, such as batteries, supercapacitors, and catalysts. This research is mainly to produce high-performance energy storage devices capable of working at high temperatures and causing no pollution in the environment. To this end, the effect of metal ion substitution on the electrochemical properties of $Co_3O_4$ for energy applications was studied. Different metal oxides, such as $FeCo_2O_4$, $MnCo_2O_4$, $Co_3O_4$, $NiCo_2O_4$, $CuCo_2O_4$, and $ZnCo_2O_4$, were synthesized using a hydrothermal process. These metal oxides were characterized using X-ray diffraction (XRD) and scanning electron microscopy (SEM), confirming the formation of phase pure materials. The electrochemical properties were studied using cyclic voltammetry (CV), galvanostatic charge-discharge techniques, and electrochemical impedance spectroscopy where it was observed that electrochemical properties of the metal oxides depend on their composition. A maximum specific capacitance of 1319 F/g at 1 mV/s was observed for $FeCo_2O_4$. Additionally, the specific capacitance of a supercapacitor device fabricated using tow $FeCo_2O_4$ electrodes were observed to decrease with an increase in scan rate and current density. The effect of temperature on energy storage capacity of the device was also investigated, and an improvement in energy storage capacity was observed with an increase in temperature, which resulted in an over 100% improvement in charge storage capacity of the supercapacitor device on increasing temperature from 10 to 70 $^oC$. It was found that

$FeCo_2O_4$ also acts as an efficient electrocatalyst for oxygen evolution reaction (OER). $FeCo_2O_4$ showed the lowest overpotential of 308 mV with the resistance of 3.4 Ohm, which was the lowest overpotential among other studied metal oxides. This work demonstrates that electrochemical properties of metal oxides can be tuned by proper metal ion substitution and could be used as advanced materials for supercapacitors and as electrocatalysts.

TABLE OF CONTENTS

LIST OF TABLES

LIST OF FIGURES

LIST OF FIGURES

# CHAPTER I

# INTRODUCTION

The increase in environmental pollution and energy consumption around the world makes necessary to use clean and efficient energy resources that can be safe, renewable, and inexpensive. Different renewable energy technologies, such as solar power, wind power, hydroelectricity, and biomass, have been used. However, to further utilize these renewable energy resources and respond to the urgent need for energy in many different weather conditions, storage devices will be needed. Therefore, it was very crucial to develop highly efficient and stable energy storage devices to meet growing demand for the energy.

## 1.1. Need and Importance of Green Energy

Currently, renewable and nuclear energy are considered to be the main alternative sources of energy production, rather than fossil fuels, which are becoming more expensive and becoming depleted. Fossil fuels also release carbon dioxide, the main gas responsible for global warming and greenhouse effects. Nuclear energy does not have these drawbacks; however, due to national security and the environmental consequences of nuclear energy, it has limited usage. The use of renewable energy is increasing rapidly. According to the U.S. Department of Energy, about 12% of the United States' energy in 2016 was from renewable sources [1].

The energy from wind, water, or sunlight is considered as green energy as these sources are environment-friendly. The most common green energy sources are wind energy, solar or thermal energy, hydropower, and biomass. According to Jaber. et al. [2], since 2000 wind and solar kept growing more rapidly more than any other energy sources. Wind power is considered as more economical due to non-requirement of fuel to operate. The main inconvenience of renewable resources is that they depend on weather conditions; for example, how much energy from the sun reaches the earth or whether the wind blows, which leads to fluctuations in energy production. Therefore, it is necessary to develop storage methods that can meet energy demands without fluctuation or intermittency [3].

## 1.2. Methods of Generating Green Energy

Energy can be generated in a variety of different ways, such as solar sources, wind energy, hydropower, and biomass energy.

### 1.2.1. Wind Energy

Wind power is the fastest growing renewable resource because of its renewability and its availability. Jaber et al. [2] mentioned that 60,000 MW is the total capacity of installing wind turbines around the world, with the production of 100 TWh per year. The concept of wind energy is to convert the kinetic energy of wind into useful power, mechanical or electrical, using rotating blades. Based on the orientation of the turbine's rotor axis, there are two basic categories of wind turbines: horizontal-axis wind turbines and vertical-axis wind turbines [4].

The major challenge of using the wind as a source of power is that the wind turbine's movement depends on weather conditions, which are unpredictable. Therefore, the generated power will be intermittent when the wind is not blowing well. Alternatively, developing an energy storage system can solve this issue [3].

### 1.2.2. Solar Energy

Solar energy can be used to get electricity using photovoltaic effect [5]. There are different ways to convert solar energy into electricity, such as solar photovoltaic systems (PV), concentrating solar power (CSP) that converts sunlight directly into electricity. These are considered to be the most useful and efficient method to generate green energy. The main limitation this technology is the amount of sunlight that reaches the earth's surface at any given time, which depends on location, geography, time of day, the season of the year, and weather conditions [6].

### 1.2.3. Hydropower

Hydropower is considered to be one of the most efficient sources for producing electric energy. It provides about 96% of the renewable energy in the United States [7]. Hydropower is one of the oldest sources of energy and produces mechanical and electrical energy using the flow of water from higher to lower elevations. The elevation and the volume of water flow determine the amount of energy produced by water moving. For example, a great deal of energy can be extracted when water flows rapidly in a large river or from a high point because it carries a great energy in its flow.

There are a few drawbacks for the hydropower. Seasonal variations such as droughts have an impact on the amount of water available for producing hydropower. In addition, hydropower has a negative impact on water wildlife, such as preventing fish migration, but this issue can be managed by constructing fish ladders [7].

### 1.2.4. Biomass Energy

Biomass energy is a renewable source of energy that is stored in plants and animals. Plants gain energy from the sun in a process called photosynthesis. Then, the chemical energy in the biomass is released as heat when it is burned; it can take the form of liquid

biofuels such as ethanol, biodiesel or biogas such as methane gas. Brown et al. [5] reported that the United States used 99 million gallons of fuel ethanol and 316 million gallons of biodiesel in 2009. Examples of biomass resources include waste food and wood, and waste materials from agricultural and industrial applications and sewage [4,6].

### 1.3. Need for Energy Storage

As energy demand is increasing all around the world due to the increase in living standards, the efficient energy storage device will be necessary to meet the growing need. Therefore, the generated energy from different energy sources must be stored so it can be available when needed. Recently, the development of renewable resources makes it more crucial to improve the storage methods because most renewable resources depend on weather conditions; thus energy production will fluctuate without an effective storage method. The storage step is becoming indispensable in order to provide an immediate response to consumer needs [9,3]. The most commonly used energy storage devices are batteries, fuel cells, and supercapacitors. Particularly, supercapacitors are considered to be one of the most effective energy storage devices due to their higher energy storage capacity, long life cycles, and fast charging. Supercapacitors' capability to discharge large amounts of power within a few seconds can meet energy surges and needs, unlike batteries [9]. The differences of power density and energy density between these devices are shown in Figure 1.1.

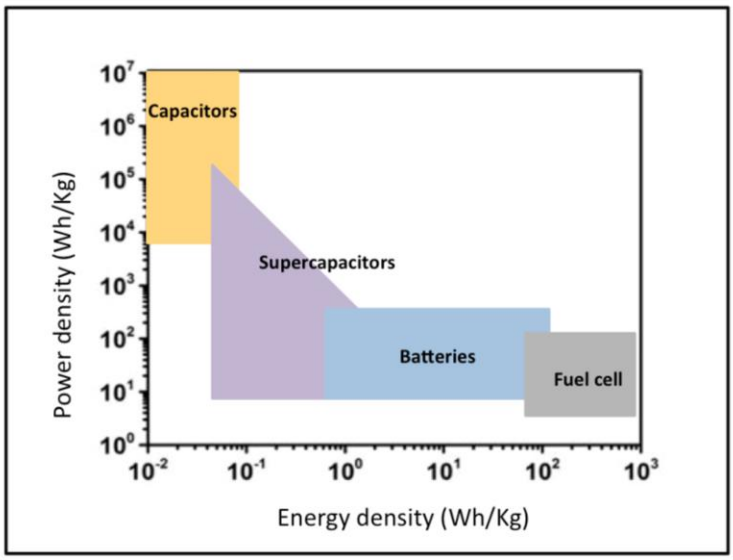


**Figure 1.1:** Energy density Power density plots for various energy storage devices.

## 1.4. Popular Energy Storage Devices

### 1.4.1. Batteries and Capacitors

A battery is a device consisting of two or more electrochemical cells that convert stored chemical energy into electrical energy. There are two types of batteries: primary batteries (disposable) and secondary batteries (rechargeable). Primary batteries, also known as traditional batteries, are simple power sources, which can be a carried and used for different purposes. Furthermore, they use electrochemical reactions of ions such as alkaline Zn-Mn, metal-air, and lithium batteries. However, these batteries have low efficiency due to the limited capacity of used materials. Rechargeable batteries are commonly used as power sources due to their capability for repeated charge and discharge. Therefore, they depend on electric current, which reverses the chemical reactions that occur during discharge, such as lithium-ion batteries. In addition, they are used in a wide range of applications, such as computer electronics devices and storage devices for solar and other renewable energy. Generally, the ideal battery should have the following characteristics: it should be inexpensive, have high energy density, and be made from the environment-

friendly material. The main performance problem of conventional batteries is the large gap between their theoretical and practical performances due to slow electrode process kinetics and low rate ionic diffusion [10].

Capacitors are energy storage devices consisting of two electrically conductive plates, which are separated by insulators called the dielectric layer. A potential difference between the two plates leads the positive charges stack to one plate and the negative charges to the other plate, which generates an electrical field as shown in Figure 1.2 where the capacitor charges storage is proportional to the potential difference (V) between the two plates; it can be calculated by the following equation:

$$C = Q/V \qquad \ldots\ldots. (1)$$

Where C is the capacitance, Q is the charge on both plate, and V is the potential applied. The low energy storage capacity limits their applications in the consumer electronics.

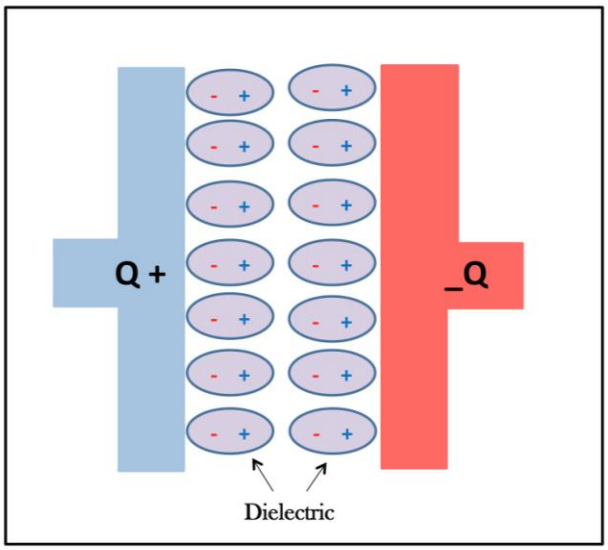


**Figure 1.2:** Capacitor aligns molecules of dielectric across an electric field to store energy

### 1.4.2. Supercapacitor

The supercapacitor, also known as an ultracapacitor, has the same principle of capacitors but instead of using insulator supercapacitors use electrolyte ionic conductor [1]. Supercapacitor based on the charge storage mechanism, supercapacitors can be divided into three types: electrical double-layer capacitance (EDLC), electrochemical pseudocapacitance and hybrid capacitance [9]. The classification of these capacitors is shown in Figure 1.3.

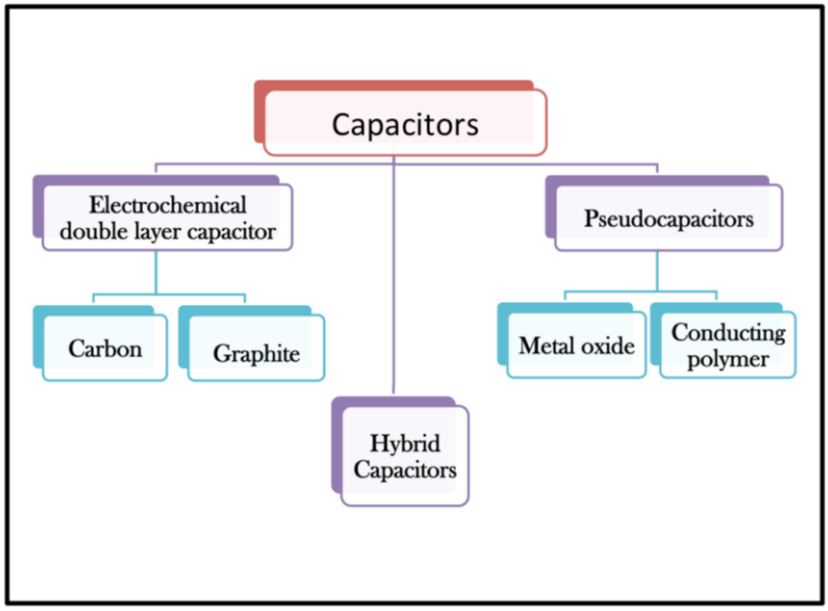


**Figure 1.3:** Types of capacitors and materials used.

#### 1.4.2.1. Electrical Double-Layer Capacitors (EDLCs)

Electrochemical double-layer capacitors are composed of two electrodes, an electrolyte, and a separator. The interfaces between the electrode and the electrolyte are the main mechanism for energy storage in EDLCs where there is no charge transfer between electrode and electrolyte (non-faradic reaction). The potential difference of the EDLCs leads the electrolyte ion to transfer to small voids in the electrode,

which produces a different polarity at the electrodes [9]. Moreover, the surface area, the electrode volumetric capacitance, the frequency behavior of the impedance, and the shape of the cyclic voltammetry must be measured in order to test the performance of EDLC electrode [12]. Thus, the capacitance is proportional to the surface area of the electrode and determined by the thickness of the separator, which can be calculated by the equation;

$$C = \frac{\epsilon A}{d} \qquad \ldots\ldots(2)$$

Where C is the capacitance, $\epsilon$ is the dielectric constant, A is the surface area ans $d$ is the distance between the two electrodes [9].

#### 1.4.2.2. Pseudocapacitors

In pseudocapacitors, the electron storage at the electrode/electrolyte is based on fast reversible oxidation/reduction reactions (faradic reaction). Some electrochemical active redox material, such as activated carbon (AC), can be added to the carbon electrode materials to increase the capacitance of a supercapacitor, which leads to ten times more capacitance than that of pure carbon-based EDLC [9]. In addition, pseudocapacitors' electrodes use two kinds of material to store a charge: (1) conducting polymers, such as polyaniline, polypyrrole, and polythiophene, and (2) metal sulfides or metal oxides. Recently, varies metal oxides such as $RuO_2$, NiO, $Fe_2O_3$, $Fe_3O_4$, and $MnO_2$ are investigated for supercapacitor applications [13].

#### 1.4.2.3. Hybrid Capacitors

Hybrid capacitors are capacitors that have properties of both electrochemical double layers and pseudocapacitors [8]. The hybrid capacitor storage principal is a dissimilar electrode, faradic (pseudocapacitors principle) and non-faradic (EDLC

principle) unlike supercapacitors, where one of the supercapacitor electrodes is substituted with a battery electrode such as lithium manganese oxide and transition metal oxide. Thus, this combination of storage mechanism enables hybrid supercapacitors to achieve energy, power densities, and cycling stability greater than either pseudocapacitors or EDLC. Wu et al. [9] reported a high energy density asymmetric $MnO_2$ nanowires and graphene with an energy density of 30.4Wh/kg, compared to those symmetrically composed of graphene/graphene (2.8 Wh/kg) and $MnO_2$/$MnO_2$ (5.2 Wh/kg). Subsequently, the asymmetric $MnO_2$/graphene cell exhibited a significant superiority in energy density. These properties make hybrid supercapacitors able to be used in a wide range of applications with lower costs such as wind power generation systems and transportation systems [9,14].

Generally, supercapacitors' advantages are that their charge and discharge process is very quick and simple compared to batteries and provides high power density as well. Also, they have very high cycle life and the charge is controllable as compared to electrochemical batteries (conventional supercapacitors). In addition, they have a wide range of operating temperatures in the range of 20 °C to 70 °C, whereas the disadvantage is that their energy density is commonly low [9].

## 1.5. Transition Metal Oxides for Energy Applications

Recently, transition metal oxides have been used as electrodes for pseudo-capacitor applications for a variety of reasons such as a large surface area, redox properties, and pore size distributions [15]. Thus, some of these metal oxides will be reviewed in details with their crucial roles in supercapacitors.

### 1.5.1. Manganese Dioxide

$MnO_2$ is widely used for energy storage applications due to its low cost and high

electrochemical performance with capability to provide a specific capacitance about 1100 F/g over a potential window of 1 V. However, manganese dioxide theoretical specific capacitances are higher than its experiment value five to ten times. More crucially, to increase the specific capacitance of $MnO_2$, the mesoporous structure of $MnO_2$ can be synthesized using different methods such as the template method, microemulsion method, and hydrothermal method. [14]. Haniam et al. [14] highlighted that semi-crystalline mesoporous $MnO_2$ synthesized using mesoporous silica KIT-6 can exhibit a capacitance of 220 F/g in a potential range from - 0.1 to - 0.55 V. Meanwhile, mesoporous $MnO_2$ prepared by a soft template method with pore size of 4–5 nm exhibited a specific capacitance of 297 F/g [14].

### 1.5.2. Cobalt Oxide:

Among different cobalt oxides, such as CoO, $Co_2O_3$, and $Co_3O_4$, $Co_3O_4$ is the most important transition metal oxide for energy storage applications. Recently, it has received greater attention because of its excellent electrochemical performance, ability to tune its electrochemical surface area and its stability. In addition, $Co_3O_4$ has a very high theoretical specific capacitance (3560 F/g). Recently studies have focused on understanding the growth mechanisms of cobalt oxide nanoparticles in order to improve its electrochemical performance, which can be enhanced by modifying the size and morphology based on the needs of the different applications. Furthermore, cobalt oxide is used for many applications such as catalysts, electronics, biomedical devices activity, and energy storage, especially in supercapacitors [15,16, 17, 18].

### 1.5.3. Nickel Cobaltite

Among the various metal oxides, $NiCo_2O_4$ possesses good electrochemical activity and electrical conductivity due to the combination of nickel and cobalt ions that

enrich the redox reactions. In addition, $NiCo_2O_4$ is low cost, low toxicity, natural abundance, and displays excellent electrochemical performance that makes it excellent energy storage material [15]. Moreover, $NiCo_2O_4$ possess the theoretical capacity of 2005 F/g in 0.6 V using an aqueous alkaline electrolyte [15]. Instead, Chang et al. [38] reported a specific capacitance of 249.8 F/g for $NiCo_2O_4$ at the current density of 0.5 A/g in1.0 M KOH.

### 1.5.4. Iron Cobalt Oxide

$FeCo_2O_4$ has been used as an electrode material for supercapacitors [21] and as an electrocatalyst. Laouini et al. studied the electrochemical behavior of $FeCo_2O_4$ thin film as a catalyst to evaluate the activity of oxygen evolution and reduction [19]. Additionally, Sharma et al. investigated the electrochemical lithium storage properties of $FeCo_2O_4$. Both studies exalt the activity of iron ion when it combines with the cobalt ion, which is considered more suitable than magnesium ion when it used as a lithium-ion battery electrode [20]. Mohamed et al. [21] reported that when $FeCo_2O_4$ is used as an anode electrode for lithium-ion battery, it provided a high capacity of 905 mAh/g at 200 mA/g current density and 16.7 F/g at a scan rate of 5 V/s.

## 1.6. Objective of the Thesis

The main objective of this research is to produce high-performance energy storage devices using cost-effective materials. Metal oxides such as $Co_3O_4$, $FeCO_2O_4$, $MnCo_2O_4$, $Co_3O_4$, $NiCo_2O_4$, $CuCo_2O_4$, and $ZnCo_2O_4$ were synthesized using a hydrothermal method for energy storage applications. The research was carried out in two phases: (1) studying the electrochemical performance of $Co_3O_4$, $FeCo_2O_4$, $MnCo_2O_4$, $NiCo_2O_4$, $CuCo_2O_4$ and $ZnCo_2O_4$ based electrodes for supercapacitors, and (2) device fabrication using the best metal oxide. In the first phase, metal oxides were synthesized

on nickel foam using the hydrothermal method followed by structural characterizations using various techniques such as X-ray diffraction (XRD) and Scanning Electron Microscopy (SEM). The electrochemical properties of the metal oxides were investigated using Cyclic Voltammetry (CV); galvanostatic charge-discharge (CD), and electrochemical impedance spectroscopy (EIS) in 3M KOH electrolyte. In the second phase, the two $FeCo_2O_4$ electrodes were used to fabricate a symmetrical supercapacitor device. The device's performance was studied electrochemically at room temperature and at various temperatures. In addition, the performance of these metal oxides as electrocatalysts for oxygen evolution reaction (OER) was studied.

# CHAPTER II

# EXPERIMENTAL

## 2.1. Materials Used

The following materials were used to prepare the metal oxides: manganese (II) nitrate tetrahydrate, $Mn(NO_3)_2.4H_2O$ (Sigma-Aldrich); iron (III) nitrate nonahydrate, $Fe(NO_3)_3.9H_2O$ (Sigma-Aldrich); and cobalt (II) nitrate hexahydrate, $Co(NO_{3)2}.6H_2O$; nickel (II) nitrate hexahydrate, $Ni(NO_3)_2.6H_2O$; copper (II) sulfate pentahydrate, $CuSO_4.5H_2O$; and zinc (II) acetate tetrahydrate, $Zn\ (CH_3COO)_2.4H_2O$ (all from Strem Chemicals). In addition, urea (Fisher Sci), isopropyl alcohol (Fisher Sci), and deionized (DI) water were used. All the materials were used without further purification. For the electrode preparation, Ni foam, poly(vinylpyrrolidone), carbon-black and N-methyl pyrrolidinone (NMP) were used.

## 2.2. Synthesis of Metal Oxides

Nanostructured metal oxides were synthesized in two steps. In the first step, the required amounts of the starting chemicals were dissolved in a mixture of DI water and isopropanol (See Table 1 for details). In this solution, urea was added. The resulting solution was stirred for 30 minutes using a magnetic stirrer and then transferred into a 45 mL Teflon-lined stainless steel autoclave. The reaction was carried out at 120 °C for a period of 12 h in an electric oven. After the hydrothermal reaction, the autoclave was

allowed to cool naturally. The precipitate was collected by centrifugation and washed with water and ethanol several times and then dried at 80 °C overnight. In the second step, the dried powder was ground and calcined at 350 °C in air for 2 h at a ramping rate of 5 °C/min to obtain the metal oxides.

**Table 2.1.** : Materials used in the synthesis of metal oxides.

| *Sample Code** | *Metal* | *$CO(NO_3)_2.6\ H_2O$* | *Urea* | *IPA* | *DI water* |
|---|---|---|---|---|---|
| MCO-84 | $Mn(NO_3)_2.4H_2O$ 0.502 g | 1.164 g | 7.2 g | 30 ml | 6 ml |
| FCO-85 | $Fe(NO_3)_3.9H_2O$ 0.808 g | 1.164 g | 7.2 g | 30 ml | 6 ml |
| CO-86 | | 1.746 g | 7.2 g | 30 ml | 6 ml |
| NCO-87 | $Ni(NO_3)_2.6H_2O$ 0.582 g | 1.164 g | 7.2 g | 30 ml | 6 ml |
| CCO-88 | $Cu\ SO_4.5H_2O$ 0.499 g | 1.164 g | 7.2 g | 30 ml | 6 ml |
| ZCO-89 | $Zn\ (CH_3COO)_2.4H_2O$ 0.439 | 1.164 g | 7.2 g | 30 ml | 6 ml |

***** MCO- $MnCo_2O_4$, FCO- $FeCo_2\ O_4$, CO-$Co_3O_4$, NCO- $NiCo_2O_4$, CCO-$CuCo_2O_4$, ZCO-$ZnCo_2O_4$.

The electrode for the electrochemical study was prepared by coating the synthesized metal oxides on the Ni foam. Before coating, Ni foam was cleaned in 3M HCl and then in DI water to remove the surface oxide layer. The Ni foam was completely dried under vacuum to remove the moisture before its weight was measured. The slurry for coating ws prepared by using 10 wt% of polyvinylidene difluoride (PVDF), 10 wt%

of activated carbon and 80 wt% of synthesized metal oxides in N-methyl pyrrolidinone (NMP). The slurry was coated on the Ni foam and dried in a vacuum oven at 60 °C.

A supercapacitor device was fabricated using two iron cobalt oxide electrodes which were separated by an ion-transporting layer (Celgard, 25μm thick, 39% porosity). A schematic diagram of the symmetric supercapacitor device is given in Figure 2.1. The electrochemical properties and performance of the device were investigated at various temperatures in 3M KOH electrolyte.

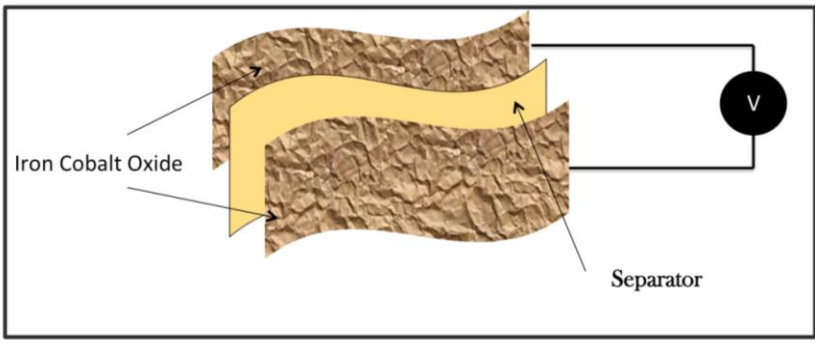


Figure 2.1: Schematic diagram of supercapacitor device.

### 2.3 Characterizations

The synthesized materials were examined using various techniques such as scanning electron microscopy, X-ray diffraction and electrochemical methods including CV, CD, EIS. More details of these characterization techniques are given below:

#### 2.3.1 X-Ray Diffraction

The phase purity and crystallographic data of the synthesized materials were investigated by X-ray diffraction using a Shimadzu X-ray diffractometer set on the 2θ-θ scan with CuKα λ=1.5406 Å radiation. The X-ray was operating at a voltage of 40 kV with a current of 30 mA. These X-rays were collimated and directed onto the sample. The measurements were conducted over the scanning angle range of 2θ = 10°−80°. An X-ray

detector was placed at an angle to satisfy the geometry so that the angle between the atomic planes and the detector was 2θ, as shown in Figure 2.2. As the sample and detector were rotated, the intensity of the reflected X-rays is recorded [22]. The slits used for source and detector were 0.2 mm.

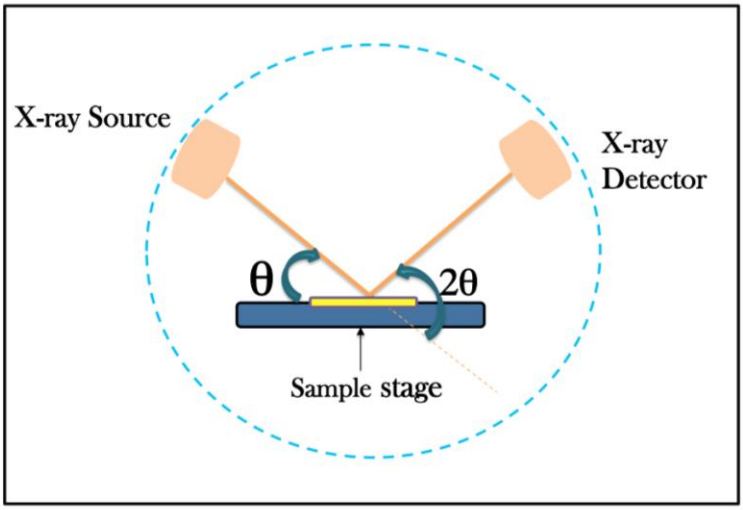


**Figure 2.2:** Schematic diagram of X-RAY diffractometer.

### 2.3.2 Scanning Electron Microscopy

The morphology of the synthesize metal oxide was observed by a field-emission scanning electron microscopy (FE-SEM). FE-SEM is a microscope that works by scanning a focused beam of electrons on a sample of interest. The electrons in the beam interact with the sample, producing various signals that can be used to obtain information about the surface topography and composition [23]. The shape and size of the particles and morphology of the samples were examined. Dr. Sanjay Mishra, at the University of Memphis, did the SEM.

### 2.3.3 Electrochemical Techniques

The electrochemical tests were performed using a standard three-electrode cell system, which contains a counter electrode, a working electrode, and a reference electrode. A platinum wire (Pt) was used as a counter electrode, saturated calomel electrode as a reference electrode, and the synthesized metal oxides coated on nickel foam were used as a working electrode. The working electrode was prepared as aforementioned by mixing 80 wt.% of the metal oxide, 10 wt.% of acetylene black and 10 wt.% of polyvinylidene difluoride (PVDF) in the presence of N-methyl pyrrolidinone (NMP) and coated on nickel foam. The schematic diagram of the three-electrode system is shown in Figure 2.3. An aqueous solution containing 3M KOH was used as an electrolyte for these electrochemical measurements. All the electrochemical measurements were performed on a Versastat 4-500 electrochemical workstation (Princeton Applied Research, USA). The electrochemical performance of metal oxides was studied by cyclic voltammetry, galvanostatic charge-discharge measurements, and electrochemical impedance spectroscopy. VersaStudio software provided by Princeton Applied Research was used for analyzing the electrochemical data.

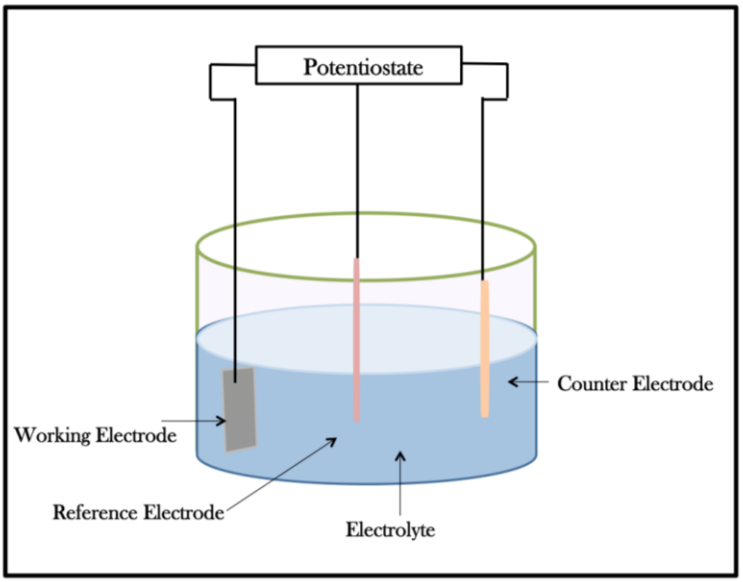


**Figure 2.3:** Schematic of three- cell electrode system.

#### 2.3.3.1 Cyclic Voltammetry (CV)

Cyclic voltammetry was used to evaluate the supercapacitor performance of the synthesized metal oxides. CV measurements were carried out in the in the potential range of 0 - 0.6 V at various scan rates (1-300 mV/s). The supercapacitor device was also tested at various scan rates at room temperature. The effect of temperature on charge storage capacity of the device was studied at a scan rate of 100 mV/s in the temperature range of 10-70 $^{o}$C.

#### 2.3.3.2 Galvanostatic Charge-Discharge Measurements

Galvanostatic charge-discharge measurements were performed to study the charge storage capacity of the synthesized metal oxides, specifically capacitance and stability. The charge-discharge studied was carried out in the potential range of 0 to 0.6 V at various applied currents. Likewise, the supercapacitor device was tested in applied discharge current of 1, 50, 100, 150, 200, 250, 300 mA/g at room temperature and at 200 mA/g in a temperature range of 10-70 $^{o}$C.

### 2.3.3.3 Electrochemical Impedance Spectroscopy

The impedance analysis of the synthesized metal oxides was conducted using an impedance analyzer in the frequency range of 0.05 to 10,000 Hz with amplitude of 10 mV. Additionally, the effect of temperature on the electrochemical behavior of the supercapacitor device was also investigated.

The application of these metal oxides as an electro catalyst for oxygen evolution reaction (OER) was also tested. The electrolysis of water could provide hydrogen, which could be used as fuel and oxygen, which could be released to the atmosphere as a breathable gas as shown in Figure 2.4. Thermodynamically, water splitting should occur at 1.23 V. However, without an efficient electro catalyst, water splitting occurs at higher potential called overpotential. The water splitting is described by the following electrochemical reactions [35]:

$2H_2O \rightarrow 2H_2 + O_2$ …..(3)

The OER activity of the metal oxide electrode was analyzed using linear sweep voltammetry at a scan rate of 1 mV/s in 1M KOH electrolyte. The electrochemical impedance spectra were also recorded to understand the charge-transport mechanism.

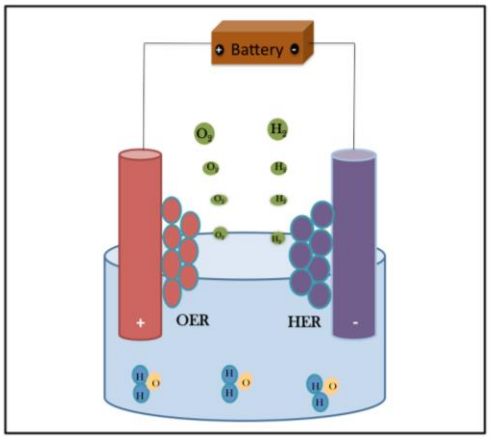


**Figure 2.4:** Schematic represents water splitting where the oxygen evolution reaction (OER) and the hydrogen evolution reaction (HER).

# CHAPTER III

# RESULTS AND DISCUSSION

## 3.1. X-ray Diffraction Analysis

Phase purity and crystallinity of the synthesized metal oxides were analyzed using powder X-ray diffraction. Figures 3.1- 3.6 show the XRD patterns of the hydrothermally synthesized $MnCo_2O_4$, $FeCo_2O_4$, $Co_3O_4$, $NiCo_2O_4$, $CuCo_2O_4$, and $ZnCo_2O_4$. The XRD pattern of $MnCo_2O_4$ shows characteristic peaks of (111), (220), (311), (400), (422), (511), (440) and (533) planes, corresponding to the cubic structure of $MnCo_2O_4$ using the standard data file (JCPDS No.23-1237). However, $FeCo_2O_4$ pattern demonstrates the peaks of (111), (220), (311), (222), (400), (422), (511), (440), and (533) planes associated with the cubic structure of $FeCo_2O_4$ given by the standard data file (JCPDS No.22-1086). The XRD peaks for the $Co_3O_4$ can be indexed to (111), (220), (311), (222), (400), (422), (511), (440), and (533) planes based on the cubic structure of $Co_3O_4$ (JCPDS 42–1467). $NiCo_2O_4$ and $CuCo_2O_4$ patterns were also matching with the standard JCPDS file for $NiCo_2O_4$ (JCPDS No.73-1702) and $CuCo_2O_4$ (JCPDS No.78-2177). The peaks observed in the $ZnCo_2O_4$ sample was indexed as (111), (220), (311), (222), (400), (422), (511) and (440) planes based on standard diffraction pattern data (JCPDS No.23-1390). No peaks other than peaks due to these metal oxides were observed in the XRD patterns of these compounds, confirming phase purity of the synthesized metal oxides.

However, Mohamed et al. [34] reported spinel $FeCo_2O_4$, $NiCo_2O_4$, and $ZnCo_2O_4$ with matching to their standard data file. Also, Manteghi et al. [17] observed a cubic phase of pure $Co_3O_4$ pattern where Pendashteh et al. [41] prepared highly order mesoporous $CuCo_2O_4$, which correspond to the pure phase. The crystallite size of the synthesized metal oxides was calculated using the XRD data using the Debye Scherrer equation [37]:

$$t = \frac{0.9\,\lambda}{\beta \cos\theta} \qquad \ldots. (4)$$

Where (t) average crystallite size, $\lambda$ is the X-ray wavelength, $\beta$ is the full width at half maximum of the diffraction line, and $\theta$ is the diffraction angle of the XRD spectra. The average crystallite size of metal oxides is listed in Table 3.1.

**Table 3.1**: The average crystallite size of metal oxides

| *Sample* | *FWHM* | *Crystallite size (nm)* |
|---|---|---|
| $MnCo_2O_4$ | 0.0158 | 15.8 |
| $FeCo_2O_4$ | 0.02215 | 23.4 |
| $Co_3O_4$ | 0.0190 | 17.5 |
| $NiCo_2O_4$ | 0.01256 | 16.3 |
| $CuCo_2O_4$ | 0.02198 | 22.9 |
| $ZnCo_2O_4$ | 0.0181 | 16.7 |

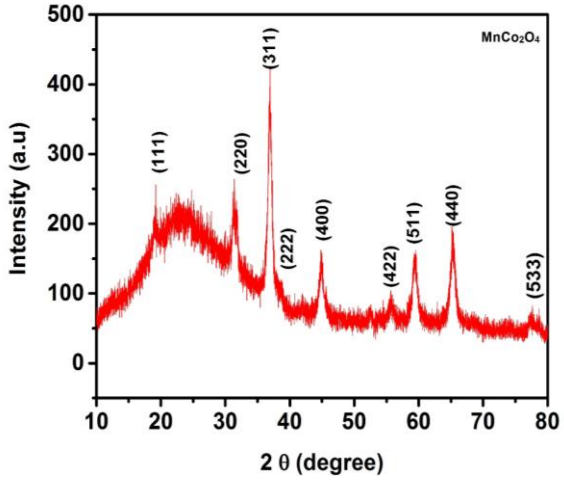


**Figure 3.1:** XRD patterns of $MnCo_2O_4$ nanostructures.

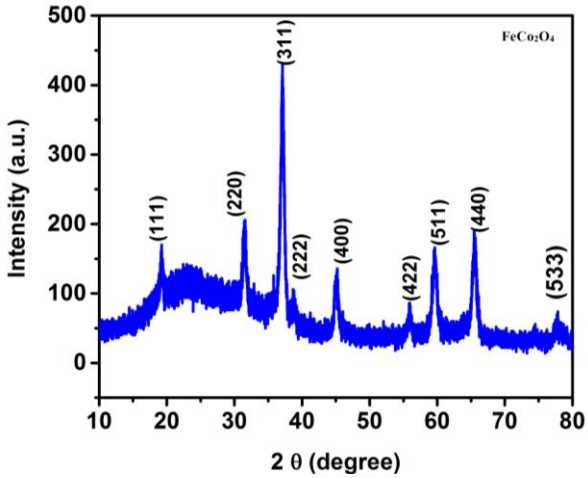


**Figure 3.2:** XRD patterns of $FeCo_2O_4$ nanostructures.

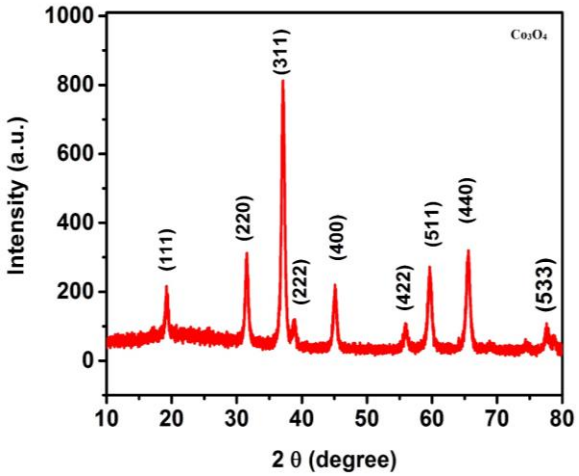


**Figure 3.3:** XRD patterns of $Co_3O_4$ nanostructures.

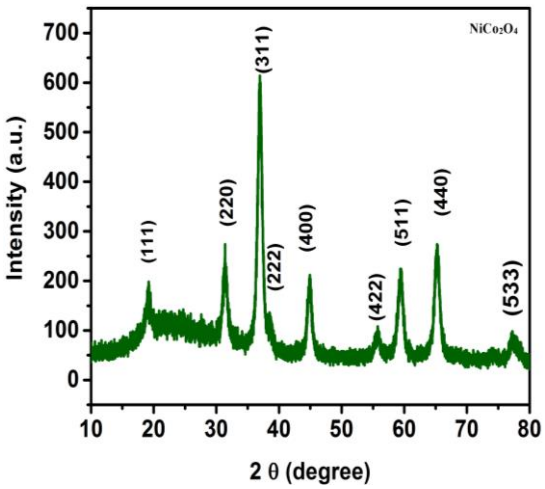


**Figure 3.4:** XRD patterns of $NiCo_2O_4$ nanostructures.

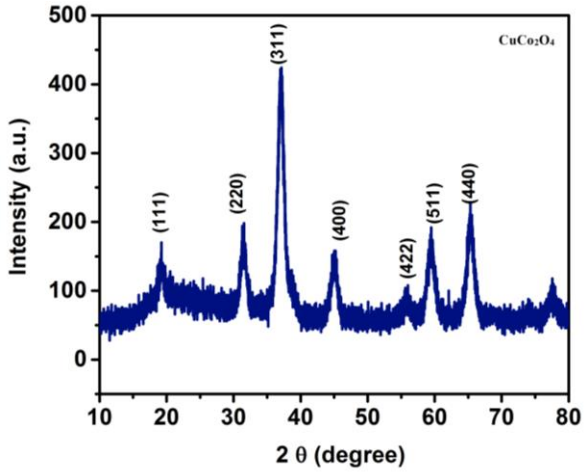


**Figure 3.5:** XRD patterns of $CuCo_2O_4$ nanostructures.

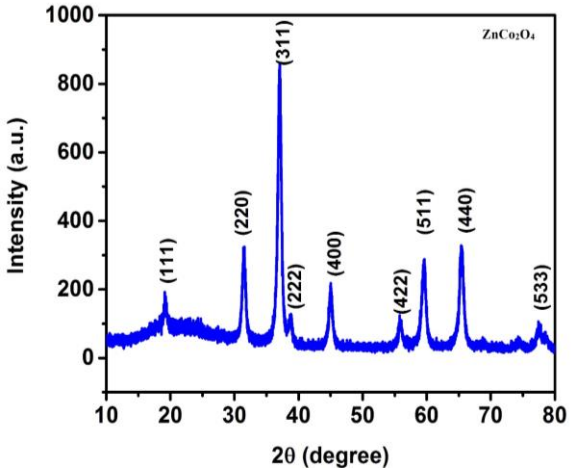


**Figure 3.6:** XRD patterns of $ZnCo_2O_4$ nanostructures.

### 3.2. Scanning Electron Microscopy Studies

The morphology and structure of the synthesized metal oxides were analyzed using scanning electron microscopy. SEM images of $FeCo_2O_4$, $CuCo_2O_4$, $NiCo_2O_4$, $Co_3O_4$, $ZnCo_2O_4$ and $MnCo_2O_4$ at different magnifications are shown in Figures 3.7 - 3.12. It was observed that morphologies of these metal oxides were nanosized, some of them were composed of many nanoparticles. In addition, the nanostructure provides a large surface area, which impacts the capacity and cycling performance [26,34].

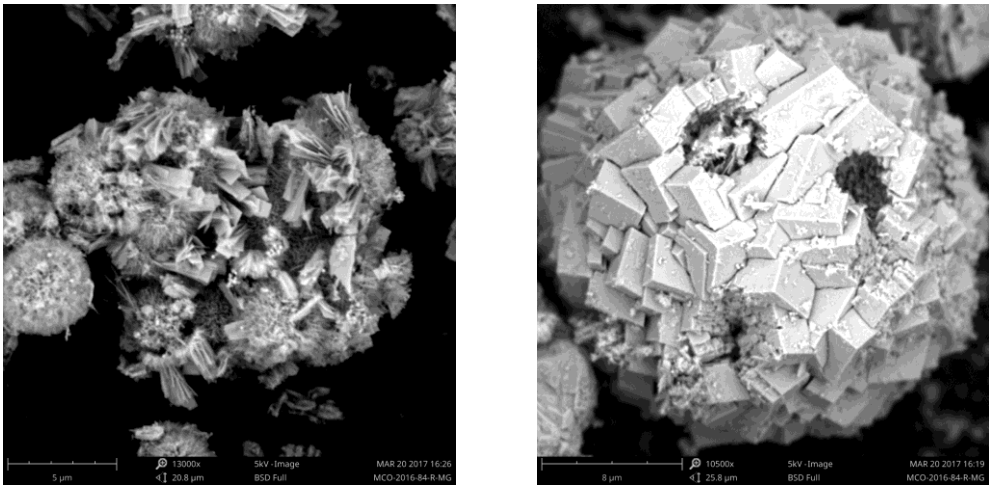


**Figure 3.7:** SEM images of $MnCo_2O_4$ at various magnifications.

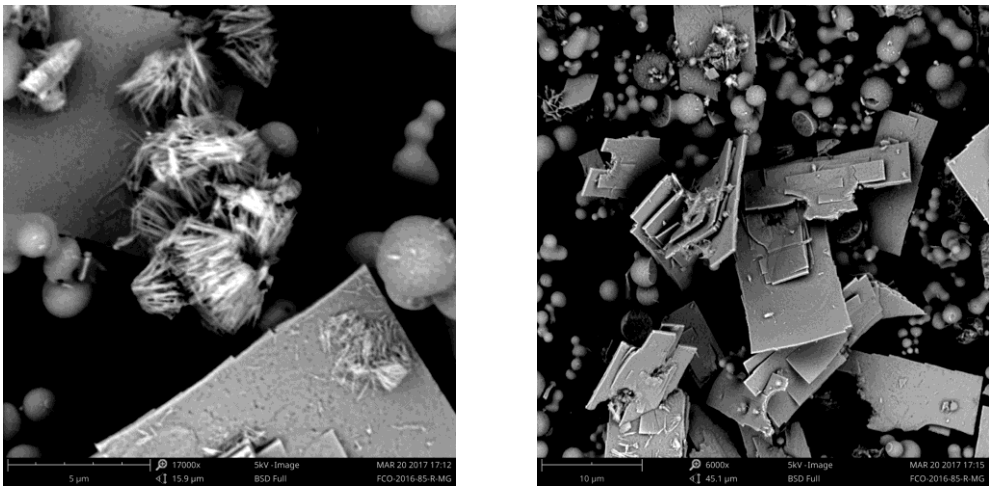


**Figure 3.8:** SEM images of $FeCo_2O_4$ at various magnifications.

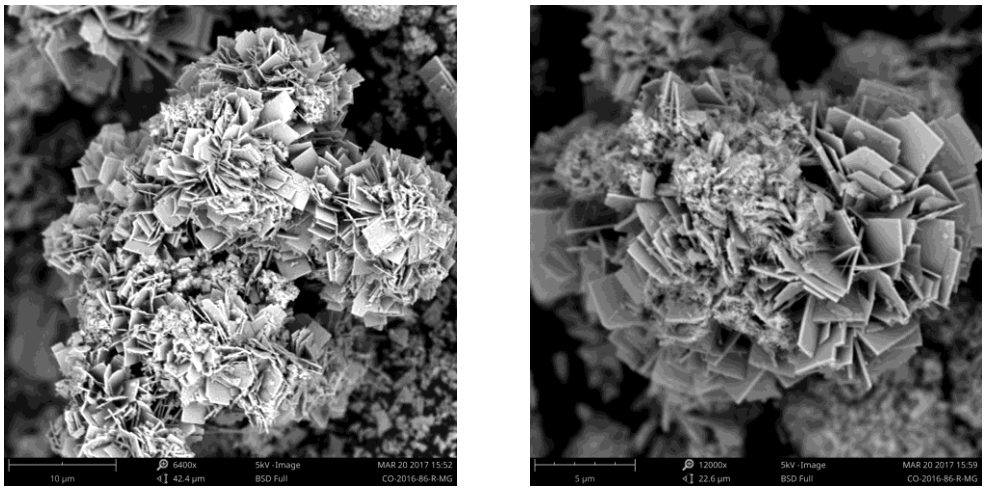


**Figure 3.9:** SEM images of $Co_3O_4$ at various magnifications.

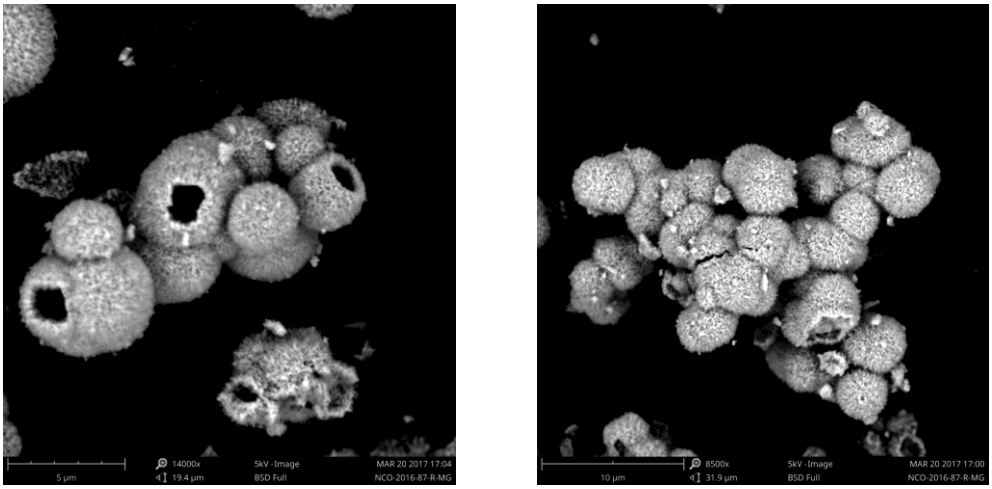


**Figure 3.10:** SEM images of $NiCo_2O_4$ at various magnifications.

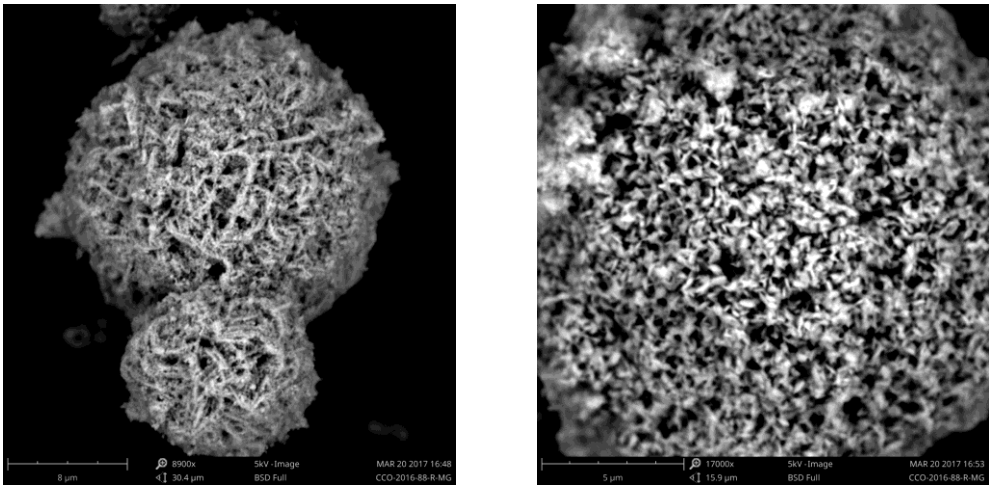


**Figure 3.11:** SEM images of $CuCo_2O_4$ at various magnifications.

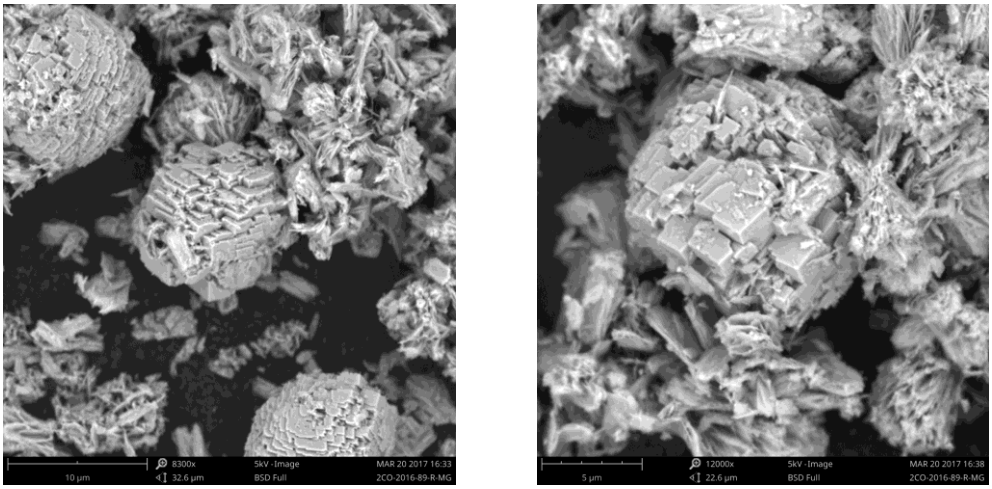


**Figure 3.12:** SEM images of $ZnCo_2O_4$ at various magnifications.

### 3.3. Electrochemical Measurements for Supercapacitors

The electrochemical performances of metal oxides were investigated in 3M KOH electrolyte using cyclic voltammetry, galvanostatic charge-discharge measurements, electrochemical impedance spectroscopy, and linear sweep voltammetry.

#### 3.3.1. Cyclic Voltammetry

Cyclic voltammograms of metal oxide electrodes in 3MKOH electrolyte were performed at various scan rates 1-300 mV/s. As seen in Figures 3.13 - 3.18, the curves were symmetric even at higher scan rates, indicating high cyclic stability in electrochemical performance [25]. Moreover, CV curves showed the redox peaks confirming faradic reaction of the metal oxides, which is the main mechanism for energy storage in this system. It was observed that the peak position shifts towards higher potential during the oxidation process and lower potentials during the reduction process as the scan rates increased from 1-300 mV/s, the peaks shifts could be associated to the conductivity and polarizability of the electrodes [26]. For example, cobalt oxide reduction peak observed at ≈ 0.55 V at a scan rate of 75 mV/s, which shifted to 0.56 V at a scan rate of 200 mV/s. The mechanism of the $Co_3O_4$ redox process in KOH electrolyte is explained by the following reaction [26]:

$$CoOOH + OH^- \rightleftharpoons CoO_2 + H_2O + e^- \quad \cdots\cdots (5)$$

$$Co_3O_4 + H_2O + OH^- \rightleftharpoons 3CoOOH + e^- \quad \cdots\cdots (6)$$

The following expression was used to calculate the specific capacitance ($C_{sp}$) of the electrodes.

$$(C_{sp}) = Q/(\Delta V \times m) \quad \ldots.(7)$$

Where Q is the area under the CV curve, ΔV is the potential, and m is the mass of the metal

oxide used in the electrode [27]. Variation of the specific capacitance as a function of scan rate for all the metal oxides is shown in Figures 3.19. It was observed that specific capacitance was decreasing with increasing scan rates, which could be due to insufficient time for the electrochemical reactions to occur at the electrode. The limited diffusion of the electrolyte ions into electrode's inner structure at high scan rate could lead to decrease the specific capacitance. The specific capacitance of all the synthesized metal oxides is listed in Table 3.2. As observed, $FeCo_2O_4$ showed the maximum specific capacitance of 1319 F/g at 1 mV/s. The specific capacitance decreased from 1319 to 120 F/g for $FeCo_2O_4$, 963 to 171 F/g for $MnCo_2O_4$, 446 to 87 F/g for $Co_3O_4$, 587 to 168 F/g for $NiCo_2O_4$, 478 to 96 F/g for $CuCo_2O_4$, and 195 to 82 F/g for $ZnCo_2O_4$ on increasing scan rate from 1 to 300 mV/s. However, Hu et al [39] have synthesized hierarchical architectures of $MnCo_2O_4$ which provided a specific capacitance of 151.2 F/g at the scan rate of 5 mV/, while mesoporous $Co_3O_4$ prepared by sol-gel method exhibited 742.3 F/g at a scan rate of 5 mV/s [40]. Hsu et al. [42] reported that spinel $NiCo_2O_4$, synthesized using thermal decomposition method, displayed a specific capacitance of 764 F/g at 2 mV/s. Moreover, according to Pendashteh et al. [41], a disordered porous $CuCo_2O_4$ exhibited a maximum specific capacitance of 260 F/g at 5 mV/s.

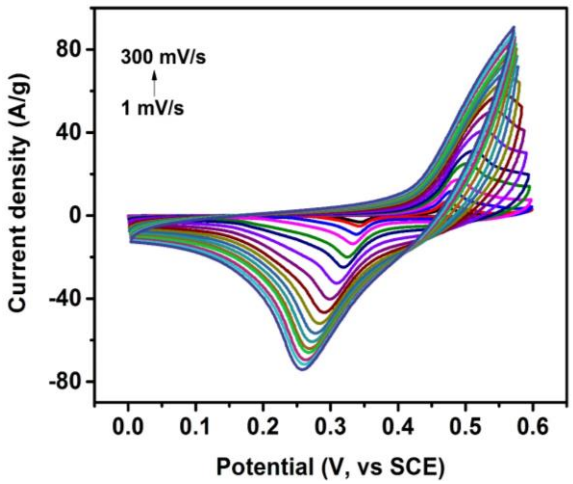


**Figure 3.13:** Cyclic voltammograms of $MnCo_2O_4$ sample at various scan rates.

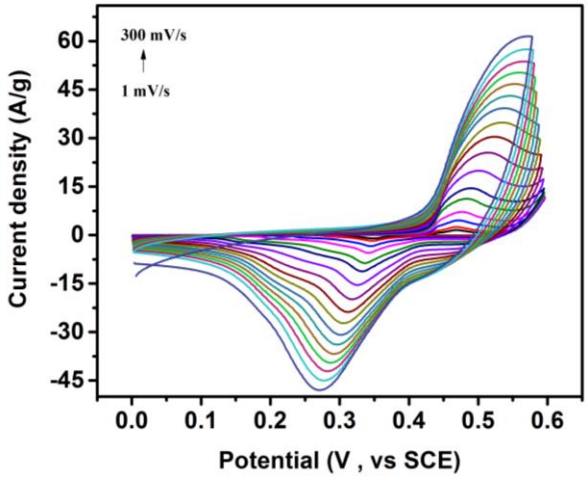


**Figure 3.14:** Cyclic voltammograms of $FeCo_2O_4$ sample at various scan rates.

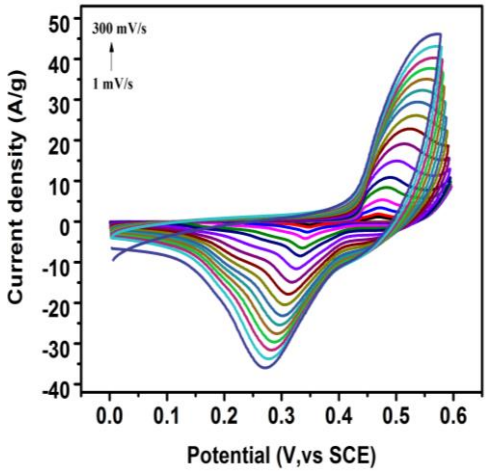


**Figures 3.15:** Cyclic voltammograms of $Co_3O_4$ sample at various scan rates.

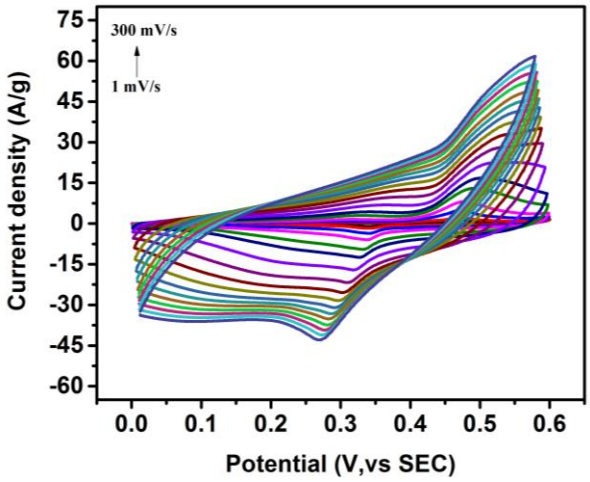


**Figure 3.16:** Cyclic voltammograms of $NiCo_2O_4$ sample at various scan rates.

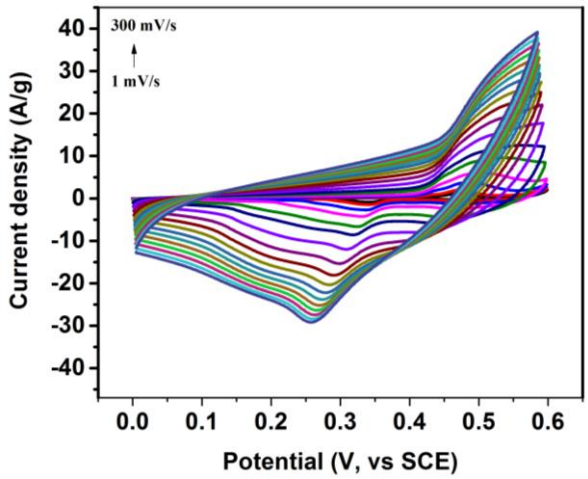


**Figure 3.17:** Cyclic voltammograms of $CuCo_2O_4$ sample at various scan rates.

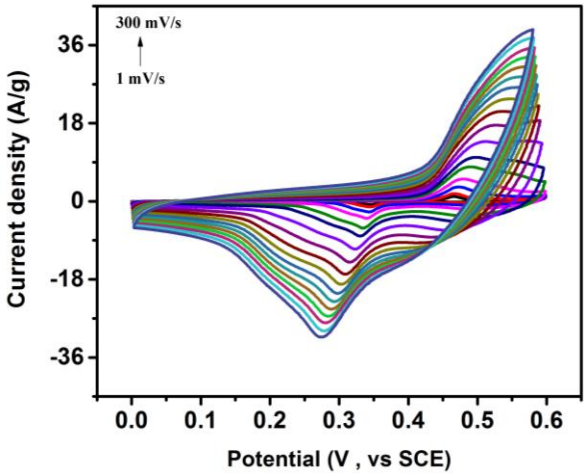


**Figure 3.18:** Cyclic voltammograms of $ZnCo_2O_4$ sample at various scan rates.

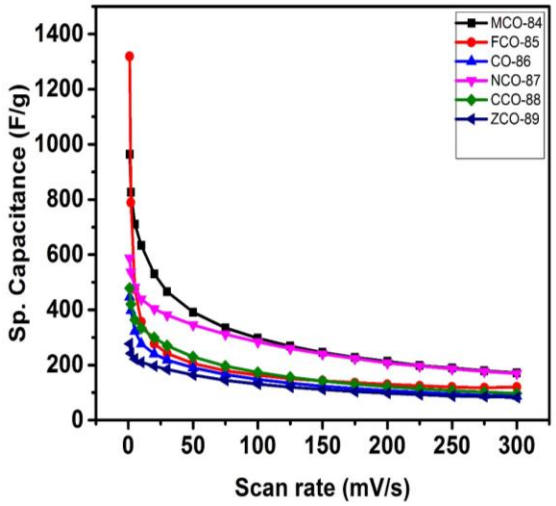


**Figure 3.19:** The variation of specific capacitance

as a function of scan rate for all the synthesized metal oxides.

**Table 3.2** : Capacity of synthesis Metal Oxides at1 mV/s scan rate

| *Metal Oxides* | *Capacity (F/g)* |
|---|---|
| $MnCo_2O_4$ | 963 |
| $FeCo_2O_4$ | 1319 |
| $Co_3O_4$ | 446 |
| $NiCo_2O_4$ | 587 |
| $CuCo_2O_4$ | 478 |
| $ZnCo_2O_4$ | 195 |

### 3.3.2. Galvanostatic Charge-Discharge

The galvanostatic charge-discharge behavior of the synthesized metal oxides was studied at various applied currents density in a potential window of 0 and 0.6 V (vs. SCE). The charge-discharge characteristics of the metal oxides electrodes are shown in Figures 3.20- 3.25. The discharge time, as shown in potential versus time curves, decreased with increase in current density, which could be due to insufficient time for the electrolytes to perform redox reactions [29]. In addition, the potential in charge-discharge curves was observed to reflect the electrodes' behavior like an ideal pseudocapacitor. This could be due to the electrochemical adsorption/desorption process at the electrode/electrolyte interface or the charge transfer reaction. Furthermore, based on the discharge curves, the specific capacitance can be calculated using the following formula [25];

$C_{sp} = (I/g \times \Delta t) / \Delta V$ ….. (8)

Where I/g is the current density (A/g), Δ t is the discharge time (s), and ΔV is the potential window (V). The variation of the specific capacitance of metal oxides versus the current density demonstrated in Figures 3.26. The specific capacitance was observed to be decreased when discharge current was increased which could be due to insufficient

time for the faradic redox reaction to occur [30]. For $FeCo_2O_4$, $CuCo_2O_4$ and $NiCo_2O_4$ electrodes there was not much change in specific capacitance with an increase in current density was observed. The rate capability of 8.6% (from 212.32 to 193.99 F/g), 15.8% (from 199.31 to 167.83 F/g) and 17.2% (from 299.01 to 247.57 F/g) was observed for $FeCo_2O_4$, $CuCo_2O_4$, and $NiCo_2O_4$ electrodes, respectively on increasing current density from 1 to 7 mA/g. Whereas, the specific capacitance of $Co_3O_4$, $ZnCo_2O_4$ and $MnCo_2O_4$ electrodes decreased with the faster increase of current density with a rate capability of 45.5% (from 235.91 to 128.48 F/g), 22.5% from 126.42 to 98.04 F/g, and 20.6% from 333.26 to 264.79 F/g. The conclusion is that the $FeCo_2O_4$ electrode kept the lowest rate capability among other oxides which makes it the best material to use in the supercapacitor application. Comparing with other reports result, $CuCo_2O_4$ nanostructures prepared using urea combustion method showed a maximum specific capacitance of 338 F/g at 1 A/g [41]. While Chang et al. [38] mentioned that $NiCo_2O_4$ electrode in KOH electrolyte provided a specific capacitance of 124.1 F/g at a current density of 1.0 A/g. Mantegh et at. reported [17] that nanostructured $Co_3O_4$ electrode maintained 90% of initial capacitance on increasing current density from 0.85 to 35 A/g. Nanowires of $MnCo_2O_4$ displayed a specific capacitance of 349.8 F /g at a current density of 1 A/g [27]. According to Liu et al. [43], $ZnCo_2O_4$ on a nickel foam showed a high specific capacitance of 1400 F/g at 1A/ g and maintained 97% of its capacitance on increasing current to 6 A/g.

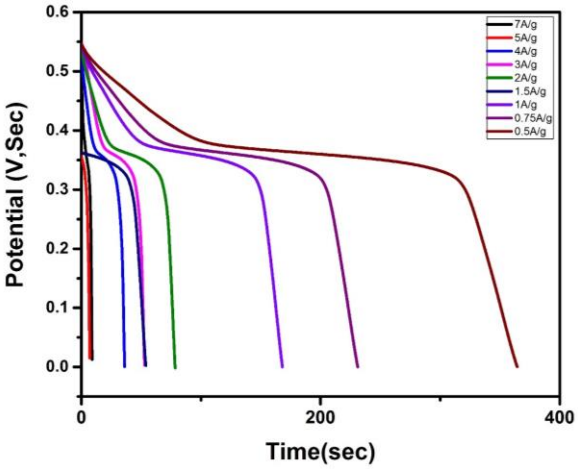


**Figure 3.20:** Galvanostatic charge-discharge of $MnCo_2O_4$ at various applied current density.

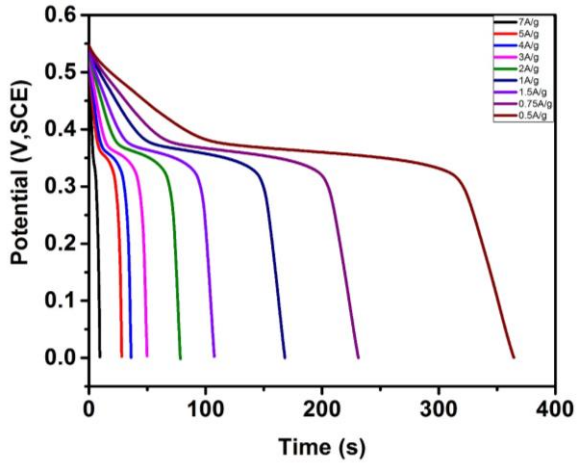


**Figure 3.21:** Galvanostatic charge-discharge of $FeCo_2O_4$ at various applied current density.

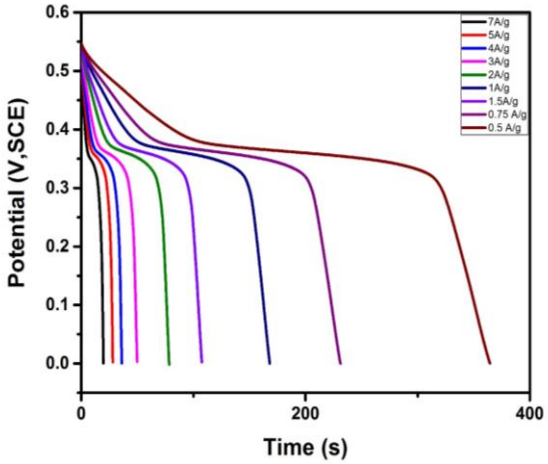


**Figure 3.22:** Galvanostatic charge-discharge of $Co_3O_4$ at various applied current density.

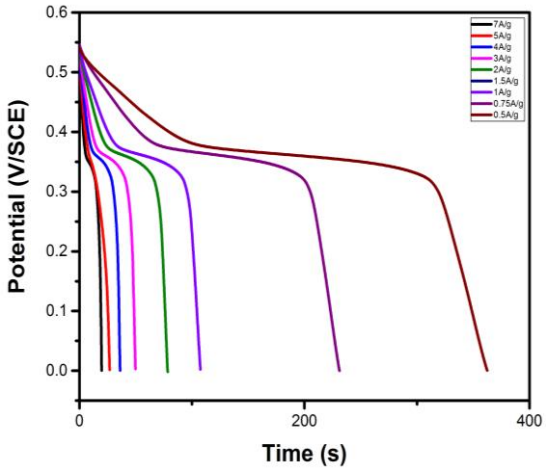


**Figure 3.23:** Galvanostatic charge-discharge of $NiCo_2O_4$ at various applied current density.

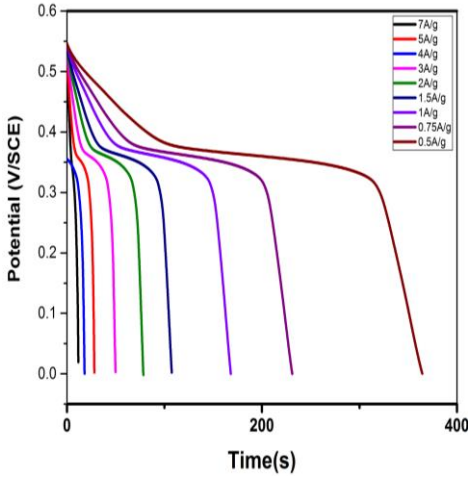


**Figure 3.24:** Galvanostatic charge-discharge of $CuCo_2O_4$ at various applied current density.

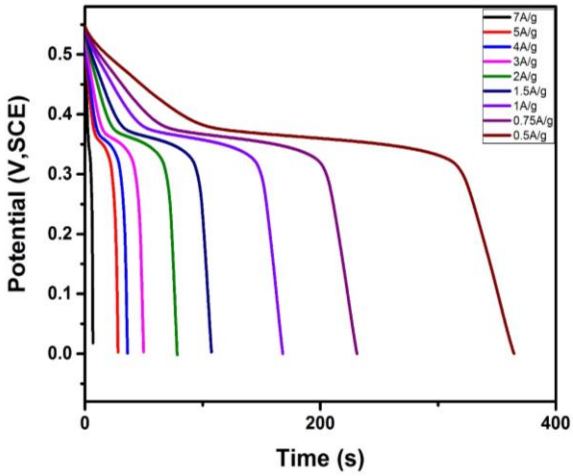


**Figure 3.25:** Galvanostatic charge-discharge of $ZnCo_2O_4$ at various applied current density.

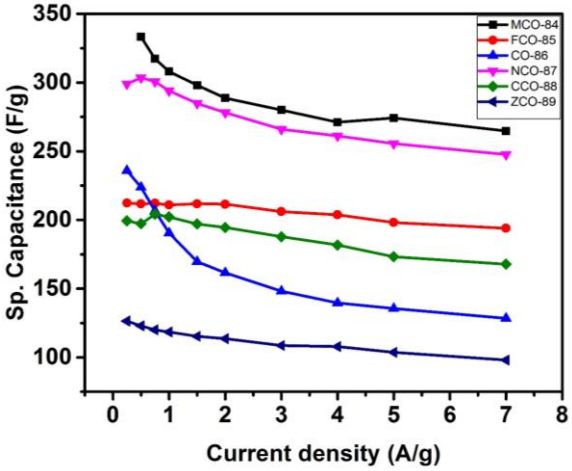


**Figure 3.26:** The variation of specific capacitance as a function of current density for all the synthesized metal oxides.

### 3.3.3. Electrochemical Behavior of the Device:

Based on the charge storage capacity of all the studied metal oxides, the $FeCo_2O_4$ electrode was selected for the fabrication of a supercapacitor device. Electrochemical measurements were performed to validate its applicability for supercapacitor application. The charge storage capacity of the supercapacitor device was studied at room temperature

and at elevated temperature. Figure 3.27 shows the cyclic voltammograms curves of the device at room temperature at various scan rates between 30-250 mV/s. The shape of the CV curves was retained even at higher scan rates, confirming high rate capability of the device. The galvanostatic charge-discharge curves of the $FeCo_2O_4$ device at various applied current densities were shown in Figure 3.28. The nature of the discharge curves are similar even at higher discharge current densities, indicating high current stability of the device. Additionally, the electrochemical impedance spectroscopy was applied to study the resistance of the $FeCo_2O_4$ device at room temperature. Figure 3.29 shows the variation of impedance as a function of frequency. It was observed that the impedance of the device decreases with increase in frequency. As well the real ($Z_{re}$) as a function of imaginary ($Z_{im}$) impedance was shown in Figure 3.30 where the real axis related to equivalent series resistance of the device.

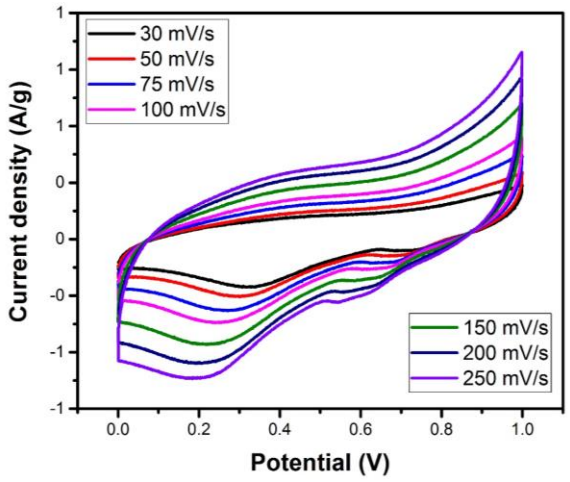


**Figure 3.27:** Room temperature cyclic voltammograms of $FeCo_2O_4$ device at various scan rates.

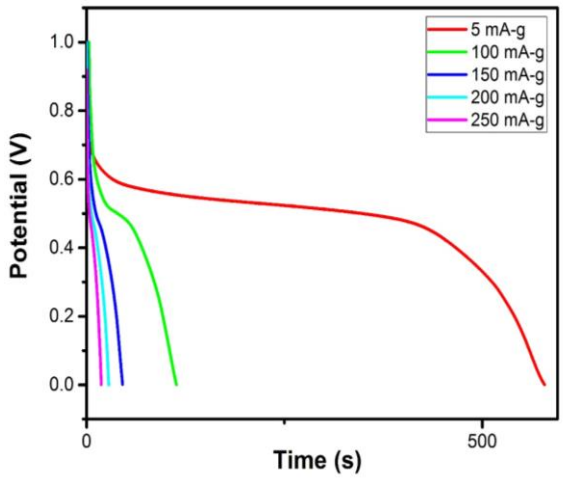


**Figure 3.28:** Room temperature galvanostatic charge-discharge characteristics of $FeCo_2O_4$ device at various applied current densities.

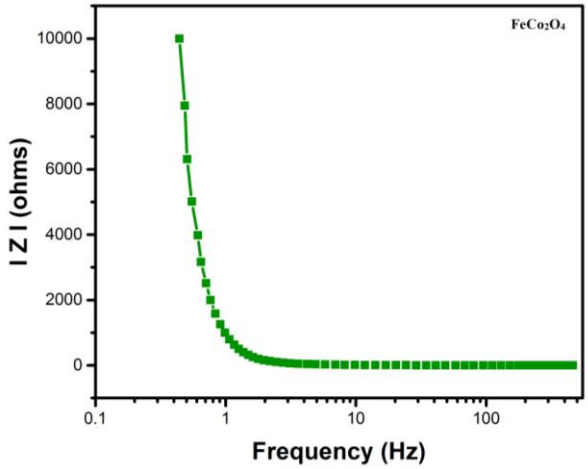


**Figure 3.29:** Variation of Z versus frequency for $FeCo_2O_4$ device at room temperature.

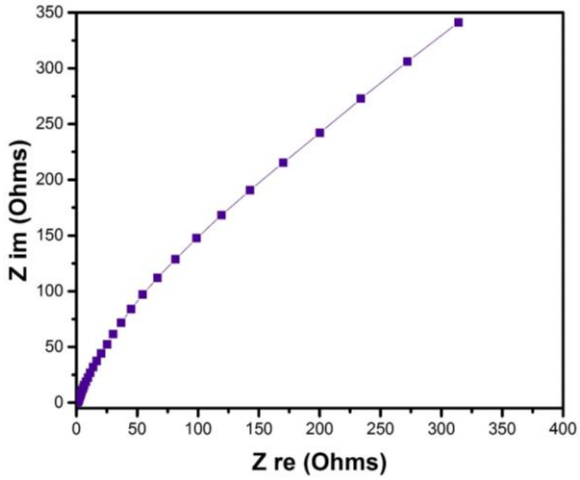


**Figure 3.30:** The variation of $Z_{re}$ and $Z_{im}$ impedance for $FeCo_2O_4$ device at room temperature.

The temperature-dependent electrochemical performance of the device was investigated as well. The cyclic voltammograms of the device at various temperatures are shown in Figure 3.31. The area under the CV curves was increased with an increase in temperature, suggesting improvement in charge storage capacity at higher temperatures. It's worth mentioning that the shape of the curve was identical in nature even at high temperatures indicating high-temperature stability of the device. The discharge time of the device was observed to be increasing with increase in temperature further confirming improvement in charge storage capacity of the device at elevated temperature as shown in Figure 3.32.

The effect of temperature on the charge storage capacity is shown in Figures 3.33 -3.34. As seen in the figures, the specific capacitance of the device increases with increasing temperature, showing over 100% improvement in the specific capacitance when the temperature was increased from 10 -70 $^{o}$C which is due to decrease in the equivalent series resistance of the device. The results suggest that charge storage capacity of the iron cobalt oxide device is higher at elevated temperatures suggesting its potential

application in high temperature applications. Electrochemical impedance spectroscopy was used to study the effect of temperature on the electrical properties of the device. As shown in Figure 3.35, the real ($Z_{re}$) and imaginary ($Z_{im}$) impedance of the device decrease with increasing temperature. The reduction in equivalent series resistance (ESR) of the device with increasing temperature demonstrates an improvement in the charge storage capacity of the device.

This decrease could be due to the enhanced mobility of the ions in the electrolyte, which increases the conductivity of the electrolyte [31]. Moreover, Figure 3.36 shows that impedance of the supercapacitor device decreases with increase in temperature and frequency.

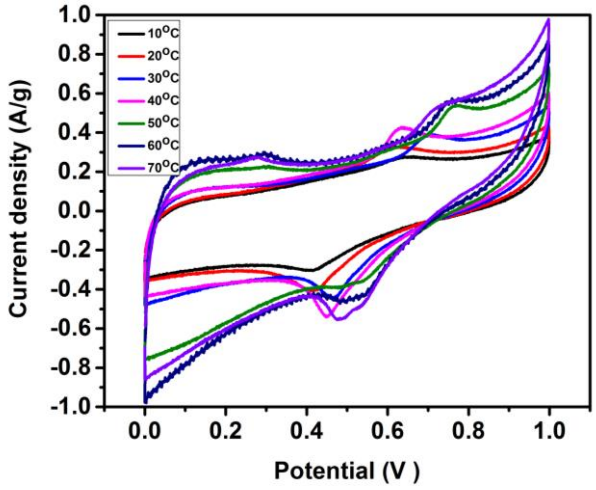


**Figure 3.31:** Cyclic voltammograms of $FeCo_2O_4$ device at various temperatures.

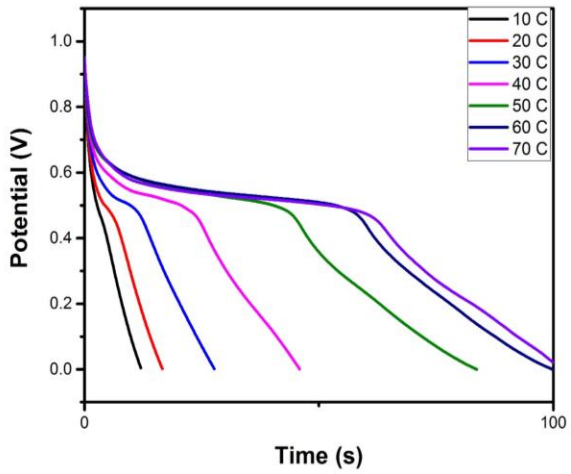


**Figure 3.32:** Galvanostatic charge-discharge curves of $FeCo_2O_4$ device at various temperatures.

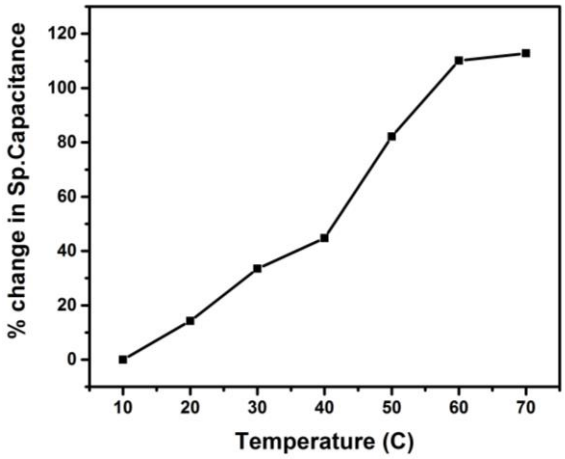


**Figure 3.33:** Effect of temperature on charge storage capacity of $FeCo_2O_4$ device determined from CV measurements.

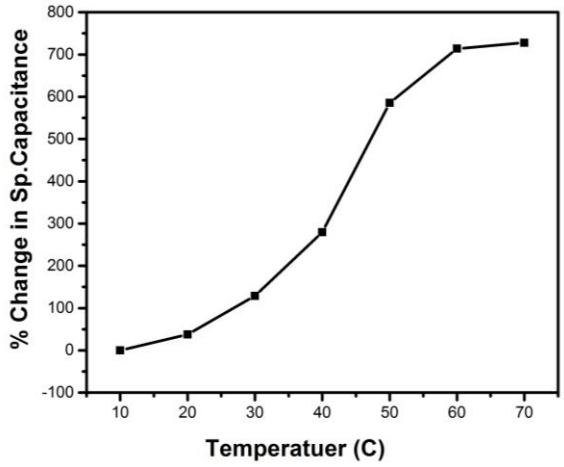


**Figure 3.34:** Effect of temperature on charge storage capacity of $FeCo_2O_4$ device determined from galvanostatic charge-discharge characteristics.

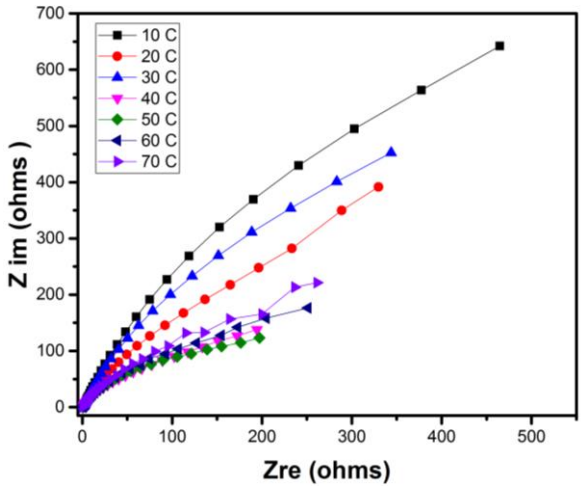


**Figure 3.35:** $Z_{re}$ vs $Z_{im}$ plots of the device at various temperatures.

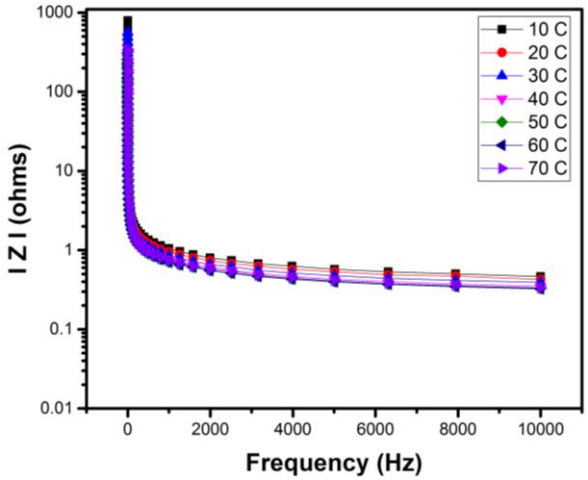


**Figure 3.36:** Variation of impedance as a function of frequency for $FeCo_2O_4$ device at various temperatures.

### 3.4. Electrochemical Measurements for Oxygen Evolution Reaction

To characterize the kinetics of the oxygen evolution reaction (OER) the linear sweep voltammetry and electrochemical impedance spectroscopy were applied.

#### 3.4.1. Linear Sweep Voltammetry

Linear sweep voltammetry was employed to study the oxygen evolution reaction using metal oxide electrodes as a catalyst in 1M KOH electrolyte. Metal oxides have been studied as OER catalysts due to their lower overpotentials for the OER at practical current, which leads to reducing the overvoltage thus enhancing the OER reaction rate [32, 33, 35]. The exhibited overpotentials for the metal oxides were observed to be 358 mV ($MnCo_2O_4$), 308 mV ($FeCo_2O_4$), 367mV ($Co_3O_4$), 367 mV ($NiCo_2O_4$), 331 mV ($CuCo_2O_4$), and 342 mV ($ZnCo_2O_4$) at 10 A/g. As seen, $FeCo_2O_4$ showed the lowest overpotential compared to other studied samples. However, OER study by Banda et al. [45] on a spinel cobalt oxide coated on nickel foam displayed a low overpotential of 244 mV at a current density of 10 $mA/cm^2$.

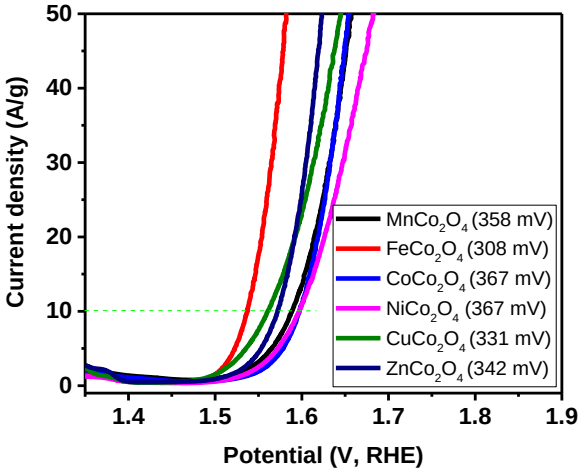


**Figure 3.37:** Polarization curves of all the samples measured at room temperature.

### 3.4.2. Electrochemical Impedance Spectroscopy

EIS measurement was employed after the linear sweep voltammetry test to study the resistance and kinetic reaction of metal oxides electrodes as a catalyst for OER over the range of frequency from $10^{-2}$ to $10^{4}$ Hz. Figure 3.38 shows the frequency versus impedance for all the samples. It was notable that $FeCo_2O_4$ has the lowest resistance of 3.4 Ω among other metal oxides electrodes. Additionally, the Nyquist plot (Figure 3.39) of all samples appeared like a semicircle, where the real axis is related to the equivalent series resistance (ESR). $FeCo_2O_4$ exhibited the lowest resistance of 3.5 Ω. It can be concluded that the $FeCo_2O_4$ works as the best electrocatalyst among the studied metal oxides for OER application.

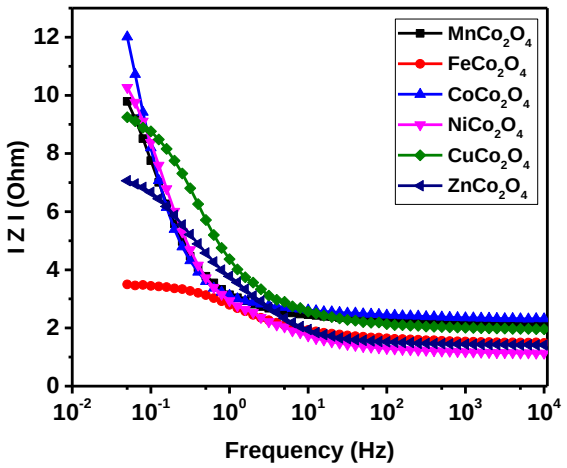


**Figure 3.38:** Variation of Z versus frequency for all the samples measured at 0.5 V (vs. SCE).

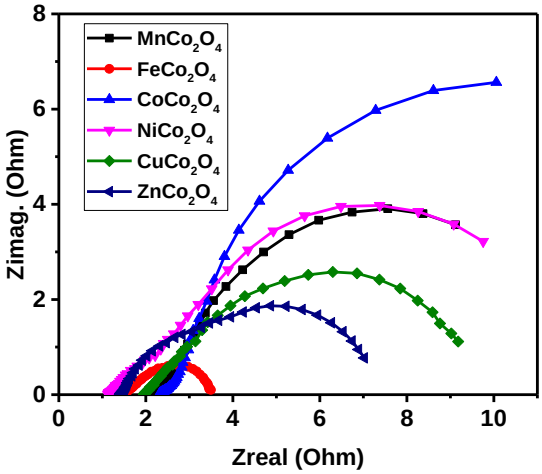


**Figure 3. 39:** Nyquist plots for all the samples measured at 0.5 V (vs. SCE).

# CHAPTER IV

# CONCLUSION

In conclusion, nanostructured metal oxides, such as $FeCo_2O_4$, $CuCo_2O_4$, $NiCo_2O_4$, $Co_3O_4$, $ZnCo_2O_4$, and $MnCo_2O_4$ were successfully synthesized using a facile hydrothermal method. The X-ray diffraction patterns of all the synthesized metal oxides matche with their standard data file suggesting high purity of the synthesized metal oxides with well defined crystalline nature. The average crystalline sizes of these nanoparticles were in the range of 15.8 to 23.4 nm.

Electrochemical tests were employed to study the supercapacitor performance of synthesized metal oxides. It was observed that the energy storage capacity depends on the composition of the metal oxides. Among studied metal oxides, iron cobalt oxide displayed the maximum charge storage capacity of 1319 F/g at 1 mV/s. In addition, iron cobalt oxide showed high rate capability. The specific capacitance of iron cobalt oxide decreased only 8.6% on increasing current density from 1 to 7 mA/g.

The symmetrical supercapacitor device that was fabricated using $FeCo_2O_4$ electrodes showed improved performance at evaluated temperatures. The specific capacitance of the devices showed over 100% improvement with increase in temperature from 10 to $70^o$ C which was due to decrease in equivalent series resistance with temperature. The OER activity of the metal oxides as an electro catalyst was investigated

using linear sweep voltammetry and electrochemical impedance spectroscopy. The $FeCo_2O_4$ electrode exhibited the lowest overpotential of 308 mV among all studied metal oxides. Our results suggest that proper composition of metals in spinal metal oxides could increase the charge storage capacity.

REFERENCES

1. Ibrahim, H.; Ilinca, A.; Perron, J. Energy Storage Systems – Characteristics and Comparisons. *Renewable and Sustainable Energy Rev.* **2008**, *12*, 1221-1250.

2. Jaber, S. Environmental Impacts of Wind Energy. *J. Clean Energy Technol*. **2013**, *1*, 251- 252.

3. Riva, G.; Foppapedretti, E.; De Carolis, C.: Giakoumelos, E.; Malametenious, C.; Signanini, P.; Giancarlo, C.; De Fazio, M. ;Gajdoš, J.; Ručinský, R. *Handbook on Renewable Energy Sources* [Online]; EnerSupply, **2011**; pp. 1-157. http://www.ener-supply.eu/downloads/ENER_handbook_en.pdf (accessed 30 August, 2017).

4. Bagher, A. M.; Vahid, M. M.; Mohsen, M. Types of Solar Cells and Application. *Amer. J. Opt. Photonics*. **2015**, *3*, 94 -113.

5. Brown, P.; Whitney, G. U.S. Renewable Electricity Generation: Resources and Challenges. Section Research Manager, 2011, 20, 1- 47.

6. U.S. Department of the Interior Bureau of Power Resources Office. *Hydroelectric Power: Managing Water in the West* [Online]; U.S. Department of the Interior: Denver, Colorado, 2011; pp. 1-334. https://www.usbr.gov/power/AssessmentReport/USBRHydro AssessmentFinalReportMarch2011.pdf (accessed 30 August, 2017).

7. Elbatran, A. H.; Abdel-Hamed, M. W.; Yaakob, O. B.; Ahmed, Y. M.; Arif Ismail, M. Hydro Power and Turbine Systems Reviews. *Jurnal Teknologi*. **2015**, *74*, 83-90.

8. Kim, B.; Sy, S.; Yu, A.; Zhang, J. Electrochemical Supercapacitors for Energy Storage and Conversion. *Handb. of Clean Energy Sys*. **2015**, 1–25.

9. Chen, J.; Cheng, F. Combination of Lightweight Elements and Nanostructured Materials for Batteries. *Acc. Chem. Res.* **2008**, *42*, 713 -718.

10. Simon, P.; Burke, A. Nanostructured Carbons: Double-Layer Capacitance and More. .*Electrochem. Soc. Interface*. **2008**, *17*, 38–43.

11. Signorelli, R.; Ku, D.C.; Kassakian, J.G.; Schindall, J.E. Electrochemical Double-Layer Capacitors Using Carbon Nanotube Electrode Structures. *Proc. IEEE*. **2009**, *97*, 1837-1847.

12. Bryan, A. M.; Santino, L. M.; Lu, Y.; Acharya, S.; D'Arcy, J. Conducting Polymers for Pseudocapacitive Energy Storage. *Chem. Mater*. **2016**, *28*, 5989-5998.

13. Deog Yoo, H.; Han, S-D.; Bayliss, R.; Gewirth, A.; Genorio, B.; Rajput, N.; Persson, K.; Burrell, A.; Cabana, J. "Rocking-Chair" Type Metal Hybrid Supercapacitors. *ACS Appl. Mater. Interfaces*, **2016**, *8*, 30853−30862.

14. Wang,Y.; Guo, J.; Wang, T.; Shao, J.; Wang, D.; Yang, Y. Mesoporous Transition Metal Oxides for Supercapacitors. *Nanomaterials.* **2015**, 1675-1676.

15. Haniam, P.; Kunsombat, C.; Songsasen A. Synthesis of Cobalt Oxides Thin Films Fractal Structures by Laser Chemical Vapor Deposition, *Sci. World J*. **2014**, 1-6

16. Yang, Q.; Lu, Z.; Sun, X.; Liu, J. Ultrathin Co3O4 Nano Sheet Arrays with High Supercapacitive Performance. *Sci. Rep*. **2013**, *3*, 1-7.

17. Manteghi, F.; Kazemi, S. H.; Peyvandipour, M.; Asghari, A. Preparation and Application of Cobalt Oxide Nanostructures as Electrode Materials for Electrochemical Supercapacitors. *RSC Adv.* **2015**, *5*, 76458-76463.

18. Wu, Z.; Zhu, Y.; Ji, X. NiCo2O4 based Materials for Electrochemical Supercapacitors. *J. of Mater. Chem. A.* **2014**, *2*, 14759–14772.

19. Laouini, E.; Berghoute,Y.; Douch,J.; Mendonça, M.H.; Hamdani, M.; Pereira, M. I. S. Electrochemical Behaviour of Fe Co O with (x = 0, 1, 2 and 3) Oxides Thin Film Electrodes x 3−x 4 in Alkaline Medium. *J. Appl. Electrochem.* **2009**, *39*, 2469−2479.

20. Sharma, Y.; Sharma, N.; Subba Rao, G. V.; Chowdari, B. V. R. Studies on Spinel Cobaltites, FeCo2O4 and MgCo2O4 as Anodes for Li-Ion Batteries. *Solid State Ionics*. **2008**, *179*, 587−597.

21. Mohamed, S.; Chen, C.; Chen, C.; Hu, S.; Liu, R. High-Performance Lithium-Ion Battery and Symmetric Supercapacitors Based on FeCo2O4 Nanoflakes Electrodes. *ACS Appl. Mater. Interfaces*. **2014**, *6*, 22701−22708.

22. Diffraction based transmission x-ray microscopy. http://www.esrf.eu/home/UsersAndScience/Publications/Highlights/highlight s-2015/enabling-technologies/et04.html (accessed 7 September, 2017).

23. How an SEM works. http://www.nanoscience.com/technology/sem-technology/how-sem-works/ (accessed 7 September, 2017).

24. Maria R. Lukatskaya1, Bruce Dunn2 & Yury Gogotsi1 .Multidimensional materials and device architectures for future hybrid energy storage. *Nature Communication*. Published 7 Sep **2016**, 1-13

25. Hu, J ; Qian, F; Song, G ;Li, W;Wang, L .Ultrafine $MnO_2$ Nanowire Arrays Grown on Carbon Fibers for High-Performance Supercapacitors. Nanoscale Research Letters, **2016**, 1-6.

26. Tummala, R; K. Guduru, R; S. Mohanty, P. Nanostructured $Co_3O_4$ electrodes for supercapacitor applications from plasma spray technique. *Journal of Power Sources*, **2012**, 44–51.

27. J. Gomez, E. E. Kalu, High-performance binder-free Co–Mn composite oxide supercapacitor electrode, J. Power Sources, 230 (**2013**) 218-224.

28. Zhao, F; Wang, Y; Xu, X; Liu, Y; Song, R; Lu, G; Li, Y. Cobalt Hexacyanoferrate Nanoparticles as a High-Rate and Ultra-Stable Supercapacitor Electrode Material, *ACS Applied Materials & Interfaces*, 6 (**2014**) 11007-11012.

29. Xie, L.-J; Wu, J.-F; Chen, C.-M; Zhang, C.-M; Wan, L,Wang, J.-L; Kong, Q.-Q; Lv, C.-X; Li, K.-X. ; Sun, G.-H. A novel asymmetric supercapacitor with an activated carbon cathode and a reduced graphene oxide–cobalt oxide nanocomposite anode. *Journal of Power Sources*, 242 (**2013**) 148-156.

30. Mitchell, E.; De Souza, F.; Gupta, R.K.; Kahol, P.K.; Kumar, D.; Dong, L.; Gupta, B.K. Probing on the Hydrothermally Synthesized Iron Oxide Nanoparticles for Ultra-Capacitor Applications, Powder Technol. **2015**, 272, 295-299.

31. Fazli, Y.; Mahdi Pourmortazavi, S.; Kohsari, I.; Sadeghpur, M. Electrochemical Synthesis and Structure Characterization of Nickel Sulfide Nanoparticles. Mater. Sci. Semicond. Process. **2014**, 27, 362–367.

32. Markovic NM, Ross PN (**2002**) Surface science studies of model fuel cell electrocatalysts. Surf Sci Rep 45:121–229.

33. Michas A, Andolfatto F, Lyons MEG, Durand R (1992) Gas evolution reactions at conductive metallic oxide electrodes for solid polymer electrolyte water electrolysis. Key Eng Mater 72–74:535–549.

34. Mohamed, S; Tsai,Y; Chen,C; Tsai, Y; Hung,T; Chang, W; Liu; R.Ternary Spinel $MCo_2O_4$ (M = Mn, Fe, Ni, and Zn) Porous Nanorods as Bifunctional Cathode Materials for Lithium−$O_2$ Batteries. ACS Appl. Mater. Interfaces **2015**, 7, 12038−12046.

35. Irshad,A ; Munichandraiah.N.High Catalytic Activity of Amorphous Ir-Pi for Oxygen Evolution Reaction.ACS Appl. Mater. Interfaces **2015**, 7, 15765−15776.

36. Kalubarme, R; Jadhav, H Ngo,D ;Park,G;Fisher, J; Choi, Y; Ryu. W;Park, C. Simple synthesis of highly catalytic carbon-free $MnCo_2O_4$@Ni as an oxygen electrode for rechargeable Li–$O_2$ batteries with long-term stability. *ScientificreportS,21 August* **2015**.1-12.

37. H. Zhang, S.C. Wang, D. Xue, Q. Chen, Z.C. Li, Preparation of Nanocrystalline $CeO_2$ by Nanocasting with Mesoporous Silica. Journal of Physics: Conference Series, **2009**, 152, 012070.

38. Chang, S; Zainal, Z ; Tan, K ; Yusof, N ; Yusoff ,W; Prabaharan, S. Synthesis and electrochemical properties ofnanostructured nickel–cobalt oxides as supercapacitor electrodes in aqueous media. I.nt. *J.Energy Res. (*2015*).* 1-12.

39. Hu J, Li W, Xu K, Zhou X, Zou R, Chen Z: Facile synthesis of porous $MnCo_2O_{4.5}$ hierarchical architectures for high-rate supercapacitors. *Cryst Eng Comm* **2014**, 16:2335–2339.

40.Wang,X.;Sumboja,A.;Khoo,E.;Yan,C.Y.;Lee,P.Cryogelsynthesisofhierarchicalinterconnected macro-/mesoporous Co3O4 with superb electrochemical energy storage. *J. Phys. Chem. C* **2012**, 116, 4930–4935.

41. Pendashteh, A; Moosavifard, S; Rahmanifar, M; Wang, Y; El-Kady, M; Kaner, R, Mousavi; M. Highly Ordered Mesoporous $CuCo_2O_4$ Nanowires, a Promising Solution

for High Performance Supercapacitors. Chem. Mater. **2015**, 27, 3919−3926

42. Hsu, C.T.; Hu, C.C. Synthesis and characterization of mesoporous spinel NiCo2O4 using surfactant-assembled dispersion for asymmetric supercapacitors. J. Power Sources **2013**, 242, 662–671.

43. Liu,B; Liu,B; Wang,Q; Wang,X; Xiang,Q; Chen,D; Shen,G. New Energy Storage Option: Toward $ZnCo_2O_4$ Nanorods/Nickel FoamArchitectures for High-Performance Supercapacitors. ACS Appl. Mater. Interfaces **2013**, 5, 10011-10017.

44. Jiang, S; Shi,T; Long,H; Sun,Y; Zhou, W; Tang, Z. High-performance binder-free supercapacitor electrode by direct growth of cobalt-manganese composite oxide nansostructures on nickel foam. Jiang et al. Nanoscale Research Letters 2014, 1-8.

45. Bandal, H; Jadhav, A; Tamboli, A; Kim,H. Bimetallic iron cobalt oxide self-supported on Ni-Foam: An efficient bifunctional electrocatalyst for oxygen and hydrogen evolution reaction. Electrochimica Acta 249 (**2017**), 253–262.